Inorganic Chemistry

Article

pubs.acs.org/IC

Tuning of the Emission Efficiency and HOMO−LUMO Band Gap for Ester-Functionalized {Al(salophen)$(H_2O)_2$}$^+$ Blue Luminophors

Virginie Béreau,*[,⊥,‡,§] Carine Duhayon,[⊥,‡] Alix Sournia-Saquet,[⊥,‡] and Jean-Pascal Sutter*[,⊥,‡]

[⊥]CNRS, LCC (Laboratoire de Chimie de Coordination), 205 Route de Narbonne, F-31077 Toulouse, France.

[‡]Université de Toulouse, UPS, INPT, LCC, F-31077 Toulouse, France

[§]IUT Paul Sabatier, Av. G. Pompidou, BP 20258, F-81104 Castres, France

Supporting Information

ABSTRACT: A series of [Al**L**$(H_2O)_2(NO_3)$] complexes, with **L** standing for an ester substituted salophen-type ligand, has been synthesized, and the luminescence properties have been investigated. These derivatives differ by the nature of the ester-R group introduced at the C5 position of their salicylidene rings (i.e., phenyl, **7a,a′**; naphthyl, **7b,b′**; pentafluorophenyl, **7c,c′**; and *p*-nitrophenyl, **7d**) and by the bis-imino bridge (i.e., 1,2- phenylene, **7a−d**; and 1,2-naphthalene, **7a′−c′**). All the complexes are characterized by luminescence in the blue range, the chemical diversity having no effect on the emission wavelength (480−485 nm). However, the emission efficiency was found to be strongly dependent on the Schiff-base ligand with quantum yields ranging from ϕ = 22% to 44%, the highest values being for the salophen derivatives with the electron-withdrawing ester-R groups (**7a**, 34%; **7a′**, 23%; **7b**, 31%; **7b′**, 22%; **7c**, 40%; **7c′**, 29%, and **7d**, 44%). Both the electrochemical data and DFT calculations show that the HOMO−LUMO band gap is modified as a function of the ester R group (from 2.92 to 3.16 eV, based on the redox potentials). The crystal structures for the *N,N′*-bis(5-(phenoxycarbonyl)salicylidene)-1,2-phenylenediamine and the *N,N′*-bis(5-(*p*-nitrophenoxycarbonyl)salicylidene)-1,2-phenylenediamine aluminum complexes (**7a** and **7d**) are reported.

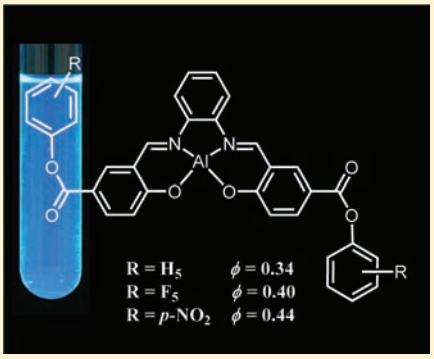

INTRODUCTION

Schiff bases, of which salen (i.e., *N,N′*-bis(salicylidene)-ethylenediamine) is the most representative example of the family, are easily prepared from condensation between an aldehyde and a primary amine. These versatile molecules are often used in coordination chemistry to complex metal ions of different sort.[1,2] One of the remarkable applications of Schiff-base complexes is in catalysis with prominent examples in the field of olefin metathesis,[3] lactide polymerizations,[4] and asymmetric oxidation.[5] Among the Schiff-base complexes are those formed with Al^{3+} that exhibit catalytic activities for oxiranes and ethylene polymerization, and for Michael addition reactions.[6] In spite of the great attention devoted to the Schiff base aluminum derivatives in catalysis, there are only very few studies devoted to their emissive properties. However, fluorescence properties for such complexes have been reported almost 40 years ago by Morisige.[7−9] Only recently, comprehensive studies on their use as luminophors,[10−12] as labeling sensors in biological systems,[13,14] and for the determination of Al^{3+} traces[15] or as materials in OLEDs[16,17] have been reported. Such a scarce examination of this family of luminophors is in obvious contrast with the extensive studies devoted to the tris(quinolato)aluminum complexes (Alq_3) which have been used as emitters, electron transporting materials, and host materials in the fabrication of OLEDs since 1987.[18]

For these two families of aluminum complexes (Schiff base and quinolate derivatives), it has been shown that the emission wavelengths can be modulated by chemical alterations at the periphery of the core of the ligand. The electron-withdrawing or electron-donating nature of substituents was found to influence the color of the emitted light for a given luminophor.[11,19,20] Another parameter of importance for potential applications as materials in OLEDs fabrication is the emission efficiency of these molecules. The design of such materials also requires the control of the HOMO and LUMO energy levels (and of the corresponding band gap) for proper alignment of these energy levels with those of other device components (charge-injection and charge-transport layers) in order to balance the mobility of the charge carriers and achieve efficient charge recombination. We have reported recently that a subtle alteration of the salophen core [i.e., the *N,N′*-bis(salicylidene)-*o*-phenylenediamine] at its periphery (the C5 position of the salicylidene rings as shown in Scheme 1) with an ester group was at the origin of a bright blue emission for aluminum complexes. Noticeable differences in the quantum yields and for the HOMO−LUMO band gaps were found as a function of the ester moiety (methanoate, *tert*-butanoate, and benzoate esters).[12] In a continuation of this first observation, we have investigated the effects of the nature of the ester R-

Received: June 6, 2011
Published: January 5, 2012

   dx.doi.org/10.1021/ic201208c | *Inorg. Chem.* 2012, 51, 1309−1318

Scheme 1. Ester Functionalized Schiff-Base Ligands

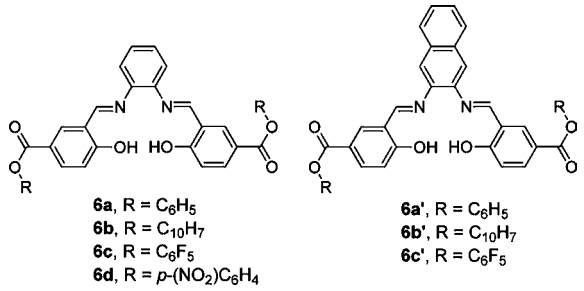

substituent and of the extent of the π-system of the ligand. We show herein that both parameters modulate significantly the emission efficiency of the complexes. For this purpose, we developed a chemical strategy for the widespread synthesis of ester-functionalized Schiff bases. This strategy focuses on the preparation of ester-functionalized salicylaldehyde derivatives that has allowed us to introduce various aromatic ester-R groups (−COOR with R = phenyl, 2-naphthyl, pentafluorophenyl, and *p*-nitrophenyl) on the salophen core. At the same time, we took advantage of this strategy to vary the extent of conjugation of the Schiff base derivatives by involving either phenylenediamine or naphthalenediamine (Scheme 1). The Al^{III} complexes of the new Schiff bases, **6b**−**d** and **6a**′−**c**′, exhibit the bright blue emission observed for complex of **6a**,[12] and enhanced quantum yields up to ϕ = 44% were obtained. Electrochemical data and DFT calculations show that the HOMO−LUMO band gap is also modified as a function of the ester R group.

RESULTS AND DISCUSSION

Synthesis and Crystal Structures. The routes for the synthesis of ester-functionalized salicylaldehydes derivatives are presented in Scheme 2. The phenyl- and 2-naphthyl-ester functionalized salicylaldehydes, respectively, **5a** and **5b**, were obtained from 3-formyl-4-hydroxybenzoic acid according to pathway 1 (a 6 step procedure). In a previous report,[12] **5a** was obtained through the reaction of 3-formyl-4-hydroxybenzoic acid with phenol and $POCl_3$ in benzene but with poor yield and in a nonreproducible way. This was attributed to the formation of polymeric materials resulting from the esterification reaction between the 3-formyl-4-hydroxybenzoic acid molecules themselves. To circumvent this drawback, we envisaged an alternative strategy by the introduction of protection/deprotection steps of the phenol group in the starting material (pathway 1). Several ether-type protecting groups have been tested, the limiting and crucial step being the deprotection that should not alter the newly introduced ester group. For this reason, benzyl ether was chosen, and intermediate **1** was obtained from the selective benzylation of the phenol group of 3-formyl-4-hydroxybenzoic acid (step i). The latter acid function was initially protected by a methyl ester, and deprotected (step ii)[21] by hydrolysis with LiOH in a methanol−water system leading to **2** with an overall yield of 82%. The esters **3a** and **3b** were obtained through a DCC-mediated coupling with a catalytic amount of DMAP and with yields no less than 80% (step iii). Cleavage of the benzyl groups in a quantitative yield was achieved in very smooth conditions by H_2 (Pd/C) with concomitant reduction of the aldehyde function (step iv). This reduction was quite surprising regarding the literature about the deprotection of benzyl ethers

Scheme 2. Synthetic Pathways for the Salicylaldehyde Derivatives 5a−d[a]

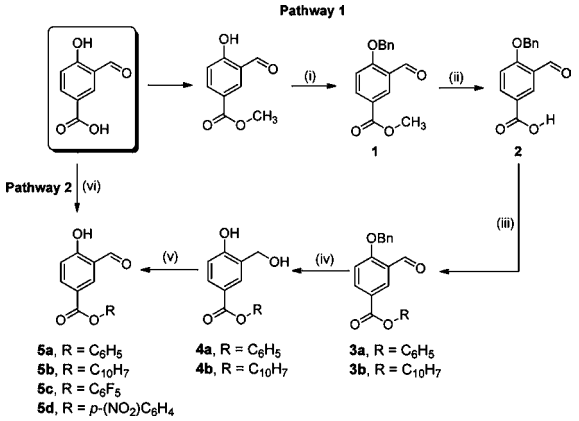

[a](i) 1 equiv BnCl, 1 equiv K_2CO_3, DMF, N_2, 85°C, overnight; (ii) 1.5 equiv $LiOH·H_2O$, MeOH/H_2O (75/25), reflux, 2h; (iii) **3a** 1 equiv phenol, 1.1 equiv DCC, 0.1 equiv DMAP, CH_2Cl_2, reflux, 4 h; **3b** 1 equiv 2-naphthol, 1.1 equiv DCC, 0.1 equiv DMAP, CH_2Cl_2, reflux, 4 h; (iv) **4a** 0.031 equiv 10% Pd/C, H_2, MeOH, RT, 3 h; **4b** 0.031 equiv 10% Pd/C, H_2, MeOH, RT, 24 h; (v) **5a** 10.4 equiv $BaMnO_4$, CH_2Cl_2, RT, 4h; **5b** 10.4 equiv $BaMnO_4$, CH_2Cl_2, RT, 24 h; (vi) **5c** 1 equiv pentafluorophenol, 1.1 equiv DCC, 0.1 equiv DMAP, CH_2Cl_2, reflux, 3 h; **5d** 1 equiv *p*-nitrophenol, 1.1 equiv DCC, 0.1 equiv DMAP, CH_2Cl_2, reflux, 3 h.

of ester-functionalized (poly)phenol[22,23] and even salicylaldehyde derivatives by hydrogenation.[24−26] Various reaction conditions (amount of catalyst, reaction time, nature of the solvent) did not change the outcomes; the only products formed were the benzyl alcohols **4a** or **4b** with some remaining starting material depending on the reaction conditions. An additional step was therefore necessary to recover the aldehyde function. The smooth oxidation with barium manganate (step v) led to **5a**/**5b**. This oxidant appeared more efficient and reliable than manganese dioxide.[27] Despite the series of protection/deprotection steps, this procedure is perfectly reproducible and more efficient, with an overall yield of almost 40%, than that reported earlier for **5a**.[12]

For the more acidic pentafluorophenol and *para*-nitrophenol, the direct DCC-mediated esterification of 3-formyl-4-hydroxybenzoic acid (Pathway 2) was straightforward with no formation of side products, yielding **5c** and **5d** in quite good yield. The formation of Schiff bases **6b**−**d** and **6a**′−**c**′ was classically operated in alcohol with the appropriate stoichiometry of the diamine (Scheme 3), as reported for **6a**.[12] Addition of $Al(NO_3)_3$ to these Schiff bases in alcohol led to the corresponding $[AlL(H_2O)_2](NO_3)$ complexes [**L** = *N*,*N*′-bis(5-naphthoxy carbonylsalicylidene)-1,2-phenylenediamine, **7b**; *N*,*N*′-bis(5-pentafluorophenoxy carbonylsalicylidene)-1,2-phenylenediamine, **7c**; *N*,*N*′-bis(5-(*p*-nitro)-phenoxy carbonylsalicylidene)-1,2-phenylenediamine, **7d**; *N*,*N*′-bis(5-phenoxycarbonylsalicylidene)-1,2-naphthalenediamine, **7a**′; *N*,*N*′-bis(5-naphthoxycarbonylsalicylidene)-1,2-naphthalenediamine, **7b**′; and *N*,*N*′-bis(5-pentafluorophenoxycarbonylsalicylidene)-1,2-naphthalenediamine, **7c**′]. All the complexes have been fully characterized by ^{1}H NMR and elemental analyses, and are very soluble in polar solvents such as alcohols, DMF, and DMSO. They are stable in air in both solid and solution states.

Single crystals suitable for X-ray analysis of the molecular structures have been obtained for the two complexes **7a** and **7d**

dx.doi.org/10.1021/ic201208c | Inorg. Chem. 2012, 51, 1309−1318

Scheme 3. Synthetic Pathways for the Ester Functionalized Schiff Bases 6a–d and 6a′–6c′ and Their Al^{3+} Complexes[a]

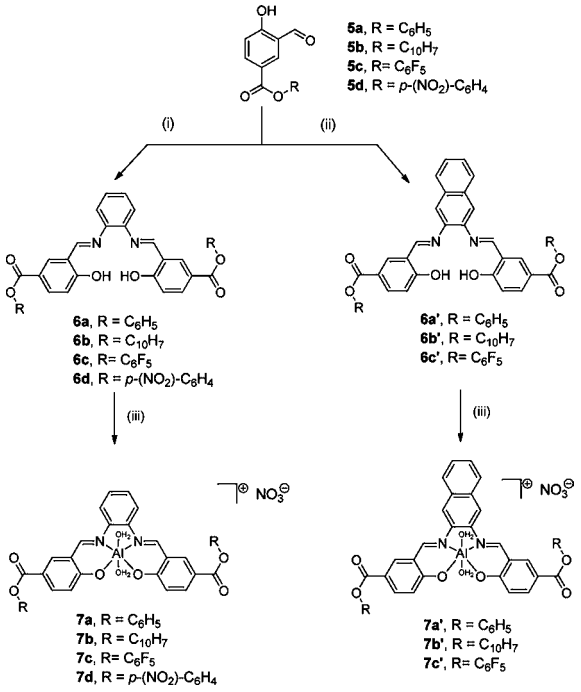

[a](i) 0.5 equiv *o*-phenylenediamine, MeOH, 3 h, RT; (ii) 0.5 equiv *o*-naphthalenediamine, MeOH, RT, 3 h; (iii) 1 equiv $Al(NO_3)_3{\cdot}9H_2O$, EtOH, refux, 3 h.

by slow evaporation of alcoholic solutions (MeOH for **7a** and EtOH for **7d**) at room temperature. The ORTEP representations of the metal complexes are shown in Figure 1; the detailed crystallographic data are summarized in Table 1.

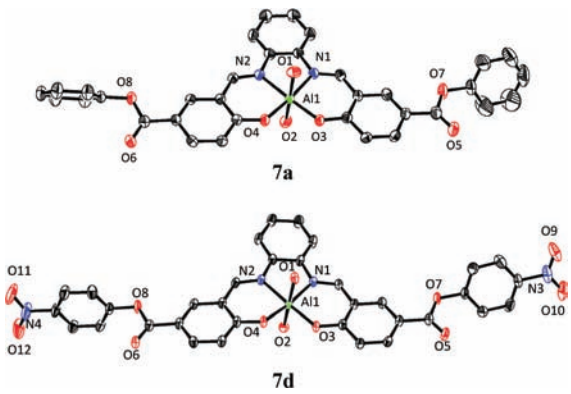

Figure 1. Molecular structures of the cationic units in **7a** and **7d** (ORTEP representation with ellipsoids at the 50% level). The nitrate anion, the H atoms, and the solvents molecules have been omitted for clarity. Selected bond lengths (Å) and angles [deg]: **7a** Al1–O1 = 1.927(3), Al1–O2 = 1.908(3), Al1–O3 = 1.821(2), Al1–O4 = 1.803(3), Al1–N1 = 1.991(3), Al1–N2 = 1.993(3), O1–Al1–O2 = 174.8(1), O3–Al1–O4 = 90.9(1), N1–Al1–N2 = 81.7(1), N1–Al1–O3 = 94.1(1), N2–Al1–O4 = 93.2(1); **7d** Al1–O1 = 1.936(2), Al1–O2 = 1.912(2), Al1–O3 = 1.832(1), Al1–O4 = 1.806(2), Al1–N1 = 1.982(2), Al1–N2 = 2.002(2), O1–Al1–O2 = 175.22(8), O3–Al1–O4 = 92.05(7), N1–Al1–N2 = 81.81(8), N1–Al1–O3 = 93.74(7), N2–Al1–O4 = 92.55(7).

Complex **7a** crystallizes in the monoclinic system and **7d** in the triclinic one. Both structures are characterized by a cationic species, the $[AlL(H_2O)_2]^+$ complex, one nitrate anion, and solvent molecules, i.e., one MeOH and two H_2O molecules for **7a**, and one and a half EtOH molecules for **7d**. The geometries of the two complexes are nearly identical with a distorted octahedral environment for the Al atom. The basal plane formed by two O atoms and two N atoms from the complexing cavity of the Schiff base (O3, O4, N1, and N2) is quite planar with the rms deviation from planarity of the atoms equal to 0.1094 and 0.0996, respectively, for **7a** and **7d**. The Al atom sits in the $[N_2O_2]$ plane in **7a** and slightly above (0.012 Å) in **7d**. The deviation from the O_h geometry is evidenced by the two Al–O bond distances (from 1.803(3) to 1.832(1) Å) shorter than the two Al–N bond distances (from 1.982(2) to 2.002(2) Å), and by the difference between the two equatorial bond angles O3–Al1–O4 and N1–Al1–N2. The two apical positions of the distorted octahedron are occupied by water molecules with Al–O bond distances longer than the equatorial Al–O bond distances (Figure 1).

Absorption, Emission, and Electrochemical Properties in Solution. The absorption and emission spectra of complexes **7a–d** and **7a′–c′** were recorded in methanol at room temperature (Figure 2). The photophysical data for absorption and emission are gathered in Table 2. All the UV–vis transitions observed for **7a–d** and **7a′–c′** are assignable to ligand-centered n–π and π–π* transitions. The UV–vis spectra feature high energy bands centered at 281, 285, 290, and 286 nm for **7a**, **7b**, **7c**, and **7d**, respectively, and at 284, 284, and 291 nm for **7a′**, **7b′**, and **7c′**, respectively. For the complexes having the bis-iminonaphthyl bridge in their structures, i.e., **7a′–c′**, this high energy band is preceded by an additional higher energy band at 264, 265, and 268 nm for **7a′**, **7b′**, and **7c′**, respectively. An intermediate absorption band with low absorbance is present around 326–332 nm; this band is not well resolved in complexes **7a′–c′**. Finally, the spectra are all characterized by a large and quite unstructured lower energy band. This absorption, detected between 372 and 376 nm for **7a–d**, is slightly red-shifted for **7a′–c′** (380–381 nm).

The room temperature luminescence spectra of complexes **7a–d** and **7a′–c′**, irradiated at 380 nm, are quite similar and display a large, unstructured band centered between 480 and 486 nm. Obviously, the nature of the ester-R group and the extent of conjugation have no influence on the emission wavelength maximum, in agreement with our preliminary observations.[12] This implies that the observed emission is salophen-centered, and involves molecular orbitals for the ground and excited singlet states that are similar for all the complexes. However, the found quantum yields clearly indicate that the emission efficiency is tuned by the nature of the ester group (Table 2). If complex **7a** with R = Ph (C_6H_5) is taken as the reference, an extension of the conjugated π system in the R group appears to have little effect on the quantum yield; values of ϕ = 34% and 31% have been obtained for, respectively, **7a** and **7b** (R = 2-naphthyl). Conversely, the presence of electron-withdrawing groups on the phenyl ring of the ester (i.e., R = C_6F_5, **7c**; and *p*-NO_2–C_6H_4, **7d**) significantly enhances the emission efficiency with ϕ = 40% for **7c** and ϕ = 44% for **7d**. The bis-imino bridge was also found to affect the efficiency of the luminescence; lower quantum yields have been obtained for the bis-iminonaphthyl-bridged compounds **7a′–c′** as compared to their bis-iminophenyl homologues **7a–c** (Table 2). Clearly, aromatic electron-withdrawing groups on the ester unit notably enhance the emission efficiency of the complexes whereas an extension of the aromatic system of the salophen core has the

dx.doi.org/10.1021/ic201208c | *Inorg. Chem.* 2012, 51, 1309–1318

Table 1. Crystallographic Data and Parameters for 7a and 7d

	7a	7d
empirical formula	$(C_{34}H_{26}AlN_2O_8)(NO_3)$, $CH_3OH,2H_2O$	$(C_{34}H_{24}AlN_4O_{12})(NO_3)$, $1.5CH_3CH_2OH$
fw	747.65	838.67
crystal size, mm^3	0.2 × 0.2 × 0.25	0.2 × 0.2 × 0.3
cryst syst	monoclinic	triclinic
space group	$P2_1/C$	$P\bar{1}$
a, Å	16.2719(2)	11.7907(3)
b, Å	15.3628(2)	12.5569(3)
c, Å	15.2615(2)	14.0286(4)
α, deg	90	87.450(2)
β, deg	114.579(2)	84.788(2)
γ, deg	90	62.541(3)
V, $Å^3$	3469.38(8)	1835.4(1)
Z	4	2
ρ_{calcd}, g cm^{-3}	1.431	1.517
μ, mm^{-1}	1.171	1.248
$F(000)$	1528	867
T, K	180	100
θ range, deg radiation (wavelength)	4.1−61.3 Cu Kα (1.541 80)	3.2−61.6 Cu Kα (1.541 80)
hkl range	−18/18, −17/17, −17/15	−13/13, −14/14, −15/15
no. reflns	26 290	204 56
unique reflns (R_{int})	5317 (0.019)	5633 (0.019)
reflns used for refinement	4565	4614
refined params	478	565
$R1$ ($I > 3\sigma(I)$)	0.0654	0.0465
wR ($I > 3\sigma(I)$)	0.0649	0.0413
GOF on F	1.000	1.259
ρ_{fin} (max/min) (e $Å^{-3}$)	1.11/−0.61	0.76/−1.31

opposite effect. It is worth noting that the quantum yields for **7c−d** compare favorably with other efficient emitters based on Al complexes.[11,20,28]

The square wave voltammetric measurements have been run in deoxygenated acetonitrile for **7a−c** and **7a′−c′**. **7d** could not be investigated because of its poor solubility. The voltammograms (Figures S1 and S2 in Supporting Information) indicate that the Al complexes undergo single irreversible oxidation and reduction. The oxidation potentials are quite high compared with those usually found (between 0.30 and 0.80 V) for neutral complexes of the same family.[11] The more difficult oxidation of compounds **7a−c** and **7a′−c′** can be related to the positive charge they are bearing; i.e., the complexes are already one electron deficient systems. Conversely, the reduction potentials have been found between −1.50 and −1.75 V indicating a rather good capability to gain an electron for **7a−c** and **7a′−c′**. The experimental HOMO and LUMO energy levels have been deduced from the redox potentials by scaling the reference (here the ferrocene/ferrocenium couple) to the zero vacuum level (Fermi level) (Table 2 and Experimental Section). While the HOMO energy levels remain almost unchanged when varying the bis-imino bridge from 1,2-phenylene (**7a**, **7b**, **7c**) to 1,2-naphthalene (**7a′**, **7b′**, **7c′**), a stabilization of the HOMO level is found by increasing the electron-withdrawing character of the phenyl ring in the ester group, from −6.21 eV for **7a** to −6.31 eV for **7c**. The same trend is found for the LUMO energy level, but the variations detected in the LUMO energy levels are more significant with −3.05 eV for **7a** to −3.25 eV for **7c**. Another noteworthy effect is related to the extent of the aromaticity of the bis-imino bridge which causes also a stabilization of the LUMO level. To gain insights into the molecular orbital diagrams and into the absorption transitions for the different Schiff-base complexes, a series of TD-DFT calculations has been undertaken.

DFT Calculations. The electronic structures of the complexes **7a−d** and **7a′−b′** were investigated by quantum chemical calculations at the TD-DFT level of theory. The geometries of **7a** and **7d** were optimized from their X-ray structures. The optimized structures show no significant differences with the solid state structures, and the angles between the planes of the aromatic R groups and the salicylidene moieties remain similar (54° and 64°, respectively, for **7a**); the only salient modification is a curvature of the ligand core for the optimized structure as compared to a perfectly planar arrangement in the solid state (Figure S3 in Supporting Information). Optimization of the geometry for **7a′**, **7b**, **7b′**, and **7c** was performed from geometry **7a** after the adequate modification of the phenyl ester group and/or the bis-iminophenyl group.

A selection of frontier molecular orbitals for **7a**, **7b′**, and **7d** are presented in Figure 3. The five highest occupied molecular orbitals and the five lowest unoccupied molecular orbitals for all compounds are given in Supporting Information (Figures S4−S9). All the MOs are exclusively ligand centered without any contribution of the metal, in agreement with earlier reports.[11,29] For **7a** and **7a′**, besides contribution of the salophen core in all MOs from HOMO to HOMO − 4, a strong involvement of the phenyl ester group is seen from the HOMO − 1 down to the HOMO − 4 with a stronger participation in the two orbitals HOMO − 2 and HOMO − 3. For the LUMO and the above orbitals, a strong contribution of the salophen core is seen; the contribution of the ester group is only slightly visible in the LUMO + 2 and LUMO + 3. For **7b** and **7b′**, the HOMO, HOMO − 1, and HOMO − 4 involve ester-based orbitals.

dx.doi.org/10.1021/ic201208c | Inorg. Chem. 2012, 51, 1309−1318

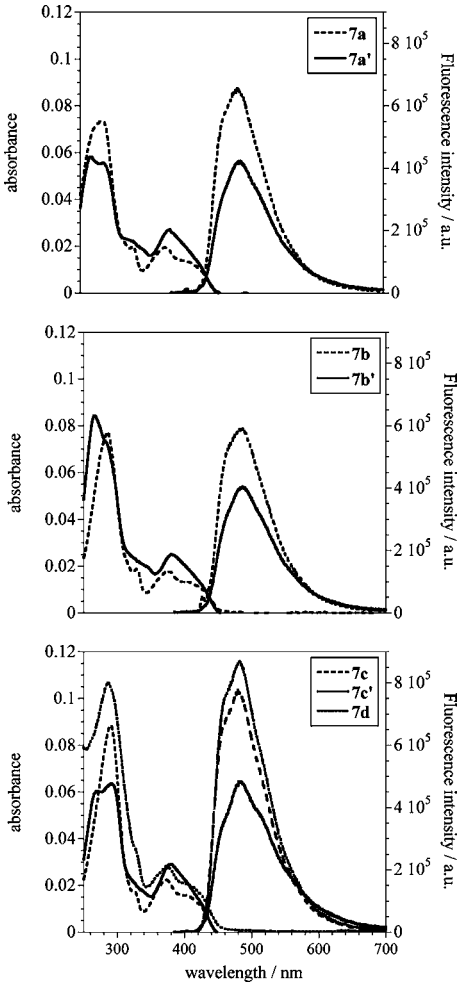

Figure 2. Absorption spectra (10^{-6} M in methanol) and emission spectra (10^{-6} M in methanol and λ_{ex} = 380 nm) of **7a**–**c** (---), **7a′**–**c′** (—), and **7d** (···).

Contribution of the salophen core is seen only in the HOMO − 2 and HOMO − 3 for **7b**, and HOMO − 2, HOMO − 3, and HOMO − 4 for **7b′**. The LUMO and LUMO + 1 for these two compounds only involve orbitals from the salophen core. Ester centered orbitals appear for higher MOs. For **7c** and **7d**, the ester contribution appears from the HOMO down to the HOMO − 4 whereas a contribution of the salophen core is seen from the HOMO down to the HOMO − 2 for **7c** and down to HOMO − 4 for **7d**. Several trends can be deduced from these molecular orbital schemes. First, the nature of the bis-imino bridge (going from **7a** to **7a′** and from **7b** to **7b′**) does not influence the distribution of the MOs. Second, a larger π system for the ester-R group (**7b** versus **7a**) and the introduction of an electron-withdrawing character on the phenyl of the ester (**7c** and **7d**) do affect the profile of the

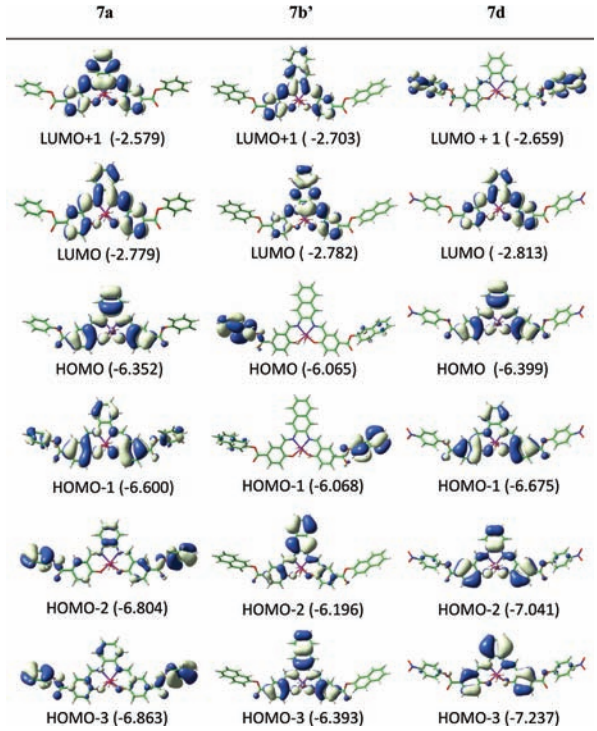

Figure 3. Selected frontier molecular orbitals for **7a**, **7b′**, and **7d**.

Table 2. Photophysical and Electrochemical Data of Complexes 7a–7d and 7a′–7c′ in Solution

	λ_{abs}[a] (logε) (nm)	λ_{em}[b] (nm)	ϕ[c]	E_g[d] (eV)	E_{ox}[e] (V)	E_{red}[e] (V)	HOMO[f] (eV)	LUMO[f] (eV)	HOMO–LUMO (eV)
7a	375 (4.30) 409 (4.11)	482	34	2.74	1.41	−1.75	−6.21	−3.05	3.16
7a′	381 (4.43) 411 (sh)	485	23	2.60	1.40	−1.55	−6.20	−3.25	2.95
7b	376 (4.24) 406 (4.11)	484	31	2.73	1.39	−1.72	−6.19	−3.08	3.11
7b′	381 (4.40) 405 (sh)	486	22	2.61	1.38	−1.60	−6.18	−3.20	2.98
7c	372 (4.36) 402 (4.18)	480	40	2.75	1.50	−1.55	−6.31	−3.25	3.06
7c′	380 (4.46) 406 (sh)	482	29	2.61	1.42	−1.50	−6.22	−3.30	2.92
7d	376 (4.43) 406 (4.32)	482	44	2.73	*g*	*g*			

[a]Measured in methanol (10^{-6} M). [b]Measured in methanol (10^{-6} M) with λ_{ex} = 380 nm. [c]ϕ in %. Quinine sulfate (ϕ = 55%) used as standard. [d]Estimated from the absorption edge. [e]The oxidation and reduction $E_{1/2}$ potentials measured in deoxygenated acetonitrile solution at room temperature. Potentials are reported against the Fc/Fc^+ couple. [f]Calculated from the E_{ox} and E_{red}. [g]Not measured because of the very poor solubility of **7d** in acetonitrile.

dx.doi.org/10.1021/ic201208c | *Inorg. Chem.* 2012, 51, 1309–1318

molecular orbitals by clearly segregating the contribution of the ester groups and of the salophen core in MOs.

The computed electronic transitions and their energies are given in Table 3 together with the experimental bands. The

Table 3. Experimental and Calculated Absorption Maximum Wavelength, Oscillator Strength (f_{calcd}), and Major Contribution of 7a−7d and 7a′−7b′

λ_{exptl}	λ_{calcd}	f_{calcd}	major contribution
7a			
281	274	0.3814	HOMO → LUMO + 2 (57%)
329	326	0.1308	HOMO − 4 → LUMO (87%)
375	365	0.3272	HOMO − 1 → LUMO (58%)
409	409	0.4433	HOMO → LUMO (98%)
7a′			
284	280	0.1848	HOMO − 8 → LUMO (90%)
327	340	0.1478	HOMO − 3 → LUMO (79%)
381	383	0.8924	HOMO − 1 → LUMO (69%)
411	395	0.2827	HOMO − 1 → LUMO + 1 (91%)
7b			
285	309	0.2960	HOMO − 6 → LUMO + 1 (65%)
329	329	0.2140	HOMO − 6 → LUMO (90%)
376	363	0.3273	HOMO − 3 → LUMO (59%)
406	406	0.3966	HOMO − 2 → LUMO (87%)
7b′			
284	305	0.0906	HOMO − 1 → LUMO + 2 (70%)
332	332	0.1134	HOMO − 7 → LUMO (66%)
381	381	0.8821	HOMO − 3 → LUMO (69%)
405	392	0.2130	HOMO − 3 → LUMO + 1 (65%)
7c			
290	278	0.3577	HOMO → LUMO + 3 (85%)
326	329	0.2451	HOMO − 2 → LUMO (100%)
372	360	0.3680	HOMO − 1 → LUMO (64%)
402	406	0.4782	HOMO → LUMO (98%)
7d			
286	302	0.1244	HOMO − 3 → LUMO+3 (68%)
329	332	0.3676	HOMO − 2 → LUMO (95%)
376	363	0.3207	HOMO − 1 → LUMO (56%)
406	407	0.5192	HOMO → LUMO (97%)

calculations show that the transitions with largest contributions to the low energy absorptions (450−350 nm) all involve MOs with a strong contribution of the salophen core. As far as the absorption close to 380 nm (the experimental excitation wavelength) is concerned, the largest contribution is from the transition HOMO − 1−LUMO for all derivatives except for **7b** and **7b′** for which the HOMO − 3−LUMO transition has the main contribution. However, in all the cases the same MO profiles are concerned. Regarding the HOMO−LUMO transitions, for **7a**, **7c**, and **7d**, they are found with a very large contribution to the band at lower energies (406−409 nm). For **7a′**, **7b**, and **7b′**, the HOMO−LUMO transition has no contribution to the band in the energy domain close to 380 nm; for these compounds, major contributions are, respectively, from HOMO − 1−LUMO + 1, HOMO − 2−LUMO, and HOMO − 3−LUMO + 1 transitions. Here again, for all the compounds, these transitions involve closely related MO profiles but with a different positioning in the respective molecular orbital diagrams.

These calculations reveal that the chemical modifications of the ligand may induce some noticeable variations in the molecular orbital diagram. However, the electronic transitions involving similar MO profiles have almost the same energies for all the compounds; only their positioning in the molecular orbital diagram is different. This allows us to understand, for instance, why the maximum emission, obtained for excitation wavelength centered at 380 nm, is same for these compounds despite chemical modifications of the ligand. We may suppose that this analogy also applies to the de-excitation pathway, hence explaining that very similar emission energies have been found for all the complexes.

The computed HOMO and LUMO energy levels are given in Figure 4 for **7a−d** and **7a′−b′**. It can be noticed that the

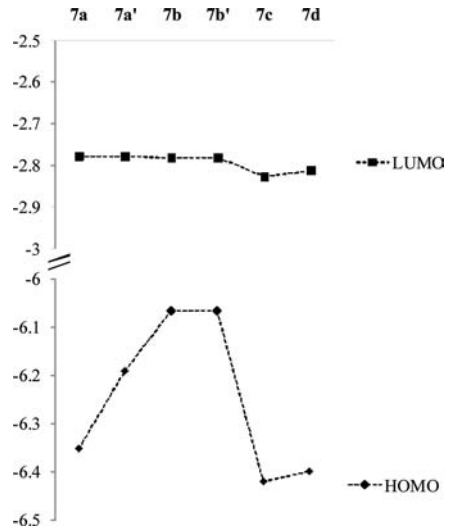

Figure 4. Calculated HOMO (◆) and LUMO (■) energy levels for **7a−d** and **7a′−b′**.

calculated LUMO energy levels only slightly vary whereas the energy level of the HOMO is more sensitive to the chemical alterations. An increase of the π system for the ester-R group (i.e., from R = phenyl, **7a**, to naphthyl, **7b**) lifts the HOMO energy level whereas imposing an electron-withdrawing character to the phenyl of the ester (in **7c** and **7d**) stabilizes the energy level of the HOMO (from −6.352 eV for **7a** to −6.420 eV for **7c** and −6.399 eV for **7d**). Such a modulation of the HOMO level without affecting the LUMO level has already been observed for 5-substituted Alq_3 complexes[19] and 5-substituted salophen complexes of aluminum.[11] Experimentally (Table 2), the LUMO was found to be more sensitive than the HOMO to the chemical modifications of the ligand. However, the HOMO−LUMO gaps suggested by the DFT calculations and those found experimentally (Table 2) follow the same trend as a function of the chemical features of the ligands.

■ CONCLUSIONS AND PERSPECTIVES

The possibility to chemically tune essential features of luminescent compounds such as emission efficiency and HOMO−LUMO band gap is of prime importance because of the prospective relevance of these materials in application such as LED. For the ester functionalized salophen complexes reported here, this is achieved simply through the ester moiety. An aromatic electron-withdrawing ester group (−COOR with R = C_6F_5 or p-NO_2−C_6H_4) was found to increase the quantum yield by 30% (from ϕ = 34% to 44%) with respect to the corresponding R = Ph derivative. The reason for the increased emission efficiencies with electron-withdrawing R groups

dx.doi.org/10.1021/ic201208c | Inorg. Chem. 2012, 51, 1309−1318

remains to be established but it might be related to charge separation considerations in the excited states.

The HOMO−LUMO band gap is also subtly modulated by the R group and by the extended aromaticity. A narrow band gap span could thus be achieved. Importantly, for this family of compounds the emission wavelength is not affected by the chemical modification at the periphery of the ligand core. For other luminophors a modification of the electronic character of the substituents has a dramatic effect on the emission wavelength.

For this study, we have also settled a straightforward synthesis strategy for ester-functionalized salicylaldehydes that allows the introduction of virtually any R at the ester function.

Future work will concern the possibility to modulate the color of emitted light by modifications of the Schiff-base core with still in mind the objective of reaching high quantum yields and adjustable HOMO−LUMO band gaps.

EXPERIMENTAL SECTION

Chemicals and General Procedures. Reagents and solvents were obtained commercially and used without further purification. (3-Formyl-4-hydroxy)benzoic acid, methyl-(3-formyl-4-hydroxy)benzoate, Schiff base **6a**, and Al^{III} complex **7a** were prepared as previously reported.[12] When specified, reactions were monitored using silica gel 60 Å analytical TLC plates by UV detection (254 nm). Silica gel (60 Å, 70−200 μm) was used for column chromatography. Elemental C, H, and N analyses were performed on a Perkin-Elmer 2400 II analyzer on freshly prepared and isolated samples

Preparations. *Methyl-(3-formyl-4-benzyloxy)benzoate (**1**).* BnCl (1.74 g; 13.72 mmol) and K_2CO_3 (1.90 g; 13.72 mmol) were added to the solution of methyl-(3-formyl-4-hydroxy)benzoate (2.47 g; 13.72 mmol) in 20 mL of dry DMF. The resulting suspension was heated under N_2 at 85 °C overnight. After cooling down at room temperature, water was added. The orange solution was extracted with CH_2Cl_2. The organic phases were washed with brine, dried over Na_2SO_4, and evaporated to dryness to give a yellow solid (3.53 g; 13.07 mmol). Yield 95%. Elemental analysis calcd (%) for $C_{16}H_{14}O_4$: C 71.10; H 5.22. Found: C 70.92; H 5.06. ^{1}H NMR (250 MHz, $(CD_3)_2CO$) δ 10.54 (1H, s, *H*C═O), 8.40 (1H, s, Ar-*H*), 8.24 (1H, d, Ar-*H*), 7.61−7.39 (6H, m, Ar-*H*), 5.44 (2H, C*H*$_2$), 3.90 (3H, s, C*H*$_3$). IR (ATR) $\nu_{C=O}$ (ester) 1716 cm^{-1}, $\nu_{C=O}$ (aldehyde) 1678 cm^{-1}.

*3-Formyl-4-benzyloxybenzoic Acid (**2**).* Methyl-(3-formyl-4-benzyloxy)benzoate **1** (0.35 g; 1.3 mmol) was solubilized in 8 mL of MeOH followed by addition of 3 mL of H_2O, leading to a cloudy solution. LiOH·H_2O (0.082 g; 1.9 mmol) was then added as solid. The suspension was refluxed until the disappearance of the precursor (around 2 h). A clear yellow solution was obtained. After evaporation of the MeOH, 35 mL of H_2O was then added. Acidification until pH 1 by addition of concentrated HCl afforded the precipitation of a white solid which was filtered and air-dried (0.285 g; 1.1 mmol). Yield 86%. Elemental analysis calcd (%) for $C_{15}H_{12}O_4$: C 70.31; H 4.72. Found: C 70.66; H 4.42. ^{1}H NMR (250 MHz, $(CD_3)_2CO$) δ 10.54 (1H, s, *H*C═O), 8.45 (1H, s, Ar-*H*), 8.27 (1H, d, Ar-*H*), 7.63−7.39 (6H, m, Ar-*H*), 5.45 (2H, C*H*$_2$). IR (ATR) $\nu_{C=O}$ (acid) 1678 cm^{-1}, $\nu_{C=O}$ (aldehyde) 1600 cm^{-1}.

*General Procedure for the Synthesis of the 4-Benzyloxy-3-formylbenzoate Derivatives **3a** and **3b**.* 3-Formyl-4-benzyloxybenzoic acid **2** (1.5 g; 5.86 mmol) was suspended in 100 mL of CH_2Cl_2. Phenol or 2-naphthol (5.86 mmol) was then added followed by the DCC (1.33 g; 6.45 mmol) leading to a clear solution. DMAP (71.6 mg; 0.586 mmol) was then added to the solution. Rapidly, a white precipitate started to appear (DCU). The mixture was refluxed for 4 h. After it was cooled down to room temperature, the solvent was evaporated. The residue was triturated with 5 mL of acetone, and the insoluble DCU was filtered. After evaporation to dryness, the yellow solid was purified by column chromatography (SiO_2, $CHCl_3$ as eluent). Data for phenyl-(4-benzyloxy-3-formyl)benzoate (**3a**) follow. Yield 79%. Elemental analysis calcd (%) for $C_{21}H_{16}O_4$: C 75.89; H 4.85. Found: C 76.13; H 4.96. ^{1}H NMR (250 MHz, $(CD_3)_2CO$) δ 10.59 (1H, s, *H*C═O), 8.58 (1H, d, Ar-*H*), 8.42 (1H, dd, Ar-*H*), 7.61−7.30 (11H, m, Ar-*H*), 5.51 (2H, s, C*H*$_2$). IR (ATR) $\nu_{C=O}$ (ester) 1720 cm^{-1}, $\nu_{C=O}$ (aldehyde) 1686 cm^{-1} . Data for 2′-naphthyl-(4-benzyloxy-3-formyl)benzoate (**3b**) follow. Yield 84%. Elemental analysis calcd (%) for $C_{25}H_{18}O_4$: C 78.52; H 4.74. Found: C 78.79; H 5.03. ^{1}H NMR (250 MHz, $(CD_3)_2CO$) δ 10.59 (1H, s, *H*C═O), 8.62 (1H, s, Ar-*H*), 8.47 (1H, d, Ar-*H*), 8.00 (3H, m, Ar-*H*), 7.83 (1H, s, Ar-*H*), 7.53 (9H, m, Ar-*H*), 5.52 (2H, s, C*H*$_2$). IR (ATR) $\nu_{C=O}$ (ester) 1717 cm^{-1}, $\nu_{C=O}$ (aldehyde) 1684 cm^{-1} .

*General Procedure for the Synthesis of the 4-Hydroxy-3-(hydroxymethyl)benzoate Derivatives **4a** and **4b**.* To a stirred solution of **3a** or **3b** (2.12 mmol) in 100 mL of MeOH (heating with a water bath around 50 °C is necessary to complete the solubilization) was added 10% Pd/C (70 mg; 0.066 mmol: 3.10% mol). The reaction vessel was air free pumped and then hydrogenated under a balloon pressure of hydrogen for 3 h for **4a** and 24 h for **4b** at room temperature. After decantation of the mixture, the supernatant was filtered through a celite pad. The solvent was then evaporated to dryness to give an oily residue which was dried under air to give a creamy white solid. Data for phenyl-(4-hydroxy-3-(hydroxymethyl))benzoate (**4a**) follow. Yield 100%. ^{1}H NMR (250 MHz, $(CD_3)_2CO$) δ 8.18 (1H, s, Ar-*H*), 7.97 (1H, d, Ar-*H*), 7.46 (2H, m, Ar-*H*), 7.28 (3H, m, Ar-*H*), 6.99 (1H, d, Ar-*H*), 4.81 (2H, s, C*H*$_2$). IR (ATR) $\nu_{C=O}$ (ester) 1728 cm^{-1} (very broad). Data for 2′-naphthyl-(4-hydroxy-3-(hydroxymethyl))benzoate (**4b**) follow. Yield 100%. ^{1}H NMR (250 MHz, $(CD_3)_2CO$) δ 8.25 (1H, s, Ar-*H*), 8.02 (4H, m, Ar-*H*), 7.78 (1H, s, Ar-*H*), 7.54 (2H, m, Ar-*H*), 7.45 (1H, d, Ar-*H*), 7.04 (1H, d, Ar-*H*), 4.76 (2H, s, C*H*$_2$). IR (ATR) $\nu_{C=O}$ (ester) 1724 cm^{-1}.

These creamy solids were used in the next step without further purification.

*General Procedure for the Synthesis of the Salicylaldehyde Derivatives **5a** and **5b**.* The corresponding 4-hydroxy-3-(hydroxymethyl)benzoate derivative **4a** or **4b** (0.4 mmol) was solubilized in 15 mL of CH_2Cl_2 (clear cream color). $BaMnO_4$ (1.07 g; 4.17 mmol) was then added, and the suspension was stirred at room temperature for 4 h for **5a** and for 24 h for **5b**. After decantation of the mixture, the supernatant was isolated. The residual solid was washed twice with 10 mL of CH_2Cl_2. These washing solutions were filtered through a celite pad. The solutions were combined and evaporated to dryness to give a brown oil. Purification of this oil was accomplished by column chromatography (SiO_2, $CHCl_3$ as eluent). Data for phenyl-(4-hydroxy-3-formyl)benzoate (**5a**) follow. Yield 55%. Elmental analysis calcd (%) for $C_{14}H_{10}O_4$: C 69.42; H 4.16. Found: C 69.65; H 4.30. ^{1}H NMR (250 MHz, $(CD_3)_2CO$) δ 10.23 (1H, s, *H*C═O), 8.66 (1H, s, Ar-*H*), 8.35 (1H, dd, Ar-*H*), 7.50 (2H, m, Ar-*H*), 7.32 (3H, m, Ar-*H*), 7.21 (1H, d, Ar-*H*). IR (ATR)

dx.doi.org/10.1021/ic201208c | *Inorg. Chem.* 2012, 51, 1309−1318

$\nu_{C=O}$ (ester) 1727 cm^{-1}, $\nu_{C=O}$ (aldehyde) 1657 cm^{-1}. Data for 2′-naphthyl-(4-hydroxy-3-formyl)benzoate (**5b**) follow. Yield 52%. Elemental analysis calcd (%) for $C_{18}H_{12}O_4$: C 73.97; H 4.14. Found: C 74.13; H 3.96. ^{1}H NMR (250 MHz, $(CD_3)_2CO$) δ 10.30 (1H, s, *H*C═O), 8.70 (1H, d, Ar-*H*), 8.40 (1H, dd, Ar-*H*), 8.01 (3H, m, Ar-*H*), 7.83 (1H, d, Ar-*H*), 7.56 (2H, m, Ar-*H*), 7.48 (1H, dd, Ar-*H*), 7.23 (1H, d, Ar-*H*). IR (ATR) $\nu_{C=O}$ (ester) 1731 cm^{-1}, $\nu_{C=O}$ (aldehyde) 1678 cm^{-1} .

*General Procedure for the Synthesis of the Salicylaldehyde Derivatives **5c** and **5d**.* 3-Formyl-4-hydroxybenzoic acid (0.5 g; 3.01 mmol) was solubilized in 25 mL of CH_2Cl_2. The corresponding phenol derivative (3.01 mmol) was then added, followed by the DCC (0.684 g; 3.31 mmol), leading to a clear solution. DMAP (37 mg; 0.303 mmol) was then added to the solution. Rapidly, a white precipitate started to appear (DCU). The mixture was refluxed for 3 h. After it was cooled down to room temperature, the insoluble DCU was filtered and the solvent removed by evaporation. Data for pentafluorophenyl-(4-hydroxy-3-formyl)benzoate (**5c**) follow. The yellow solid was purified by column chromatography (SiO_2, $CHCl_3$ as eluent). Yield 65%. Elemental analysis calcd (%) for $C_{14}H_5F_5O_4$: C 50.62; H 1.52. Found: C 50.86; H 1.38. ^{1}H NMR (250 MHz, $CDCl_3$) δ 10.04 (1H, s, *H*C═O), 8.52 (1H, d, Ar-*H*), 8.36 (1H, dd, Ar-*H*), 7.18 (1H, d, Ar-*H*). IR (ATR) $\nu_{C=O}$ (ester) 1750 cm^{-1}, $\nu_{C=O}$ (aldehyde) 1666 cm^{-1}. Data for *p*-nitrophenyl-(4-hydroxy-3-formyl)benzoate (**5d**) follow. The yellow solid was washed several times with acetone until there is no more precipitation of DCU. The yellow oil was washed with CH_2Cl_2 to yield a cream solid. Yield 65%. Elemental analysis calcd (%) for $C_{14}H_9NO_6$: C 58.54; H 3.16; N 4.88. Found: C 58.41; H 3.42; N 4.89. ^{1}H NMR (250 MHz, $CDCl_3$) δ 10.25 (1H, s, *H*C═O), 8.70 (1H, d, Ar-*H*), 8.42 (3H, m, Ar-*H*), 7,67 (2H, d, Ar-*H*), 7.22 (1H, d, Ar-*H*). IR (ATR) $\nu_{C=O}$ (ester) 1731 cm^{-1}, $\nu_{C=O}$ (aldehyde) 1656 cm^{-1}.

*General Procedure for the Preparation of Schiff Bases **6a**′, **6b**–**b**′, **6c**–**c**′, and **6d**.* The corresponding salicylaldehyde derivative **5a**–**d** (0.330 mmol) was solubilized in 4 mL of MeOH. To this clear colorless solution was dropwise added the diamine solution (0.165 mmol in 4 mL of MeOH). The resulting solution turned bright yellow to orange. A yellow precipitate started to appear during the stirring of the solution at room temperature. After 3 h, the yellow solid was filtered and dried under vacuum.

*N,N′-Bis(5-(phenoxycarbonyl)salicylidene)-1,2-naphthalenediamine (**6a**′).* Yield: 80%. Elemental analysis calcd (%) for $C_{38}H_{26}N_2O_6{\cdot}0.5H_2O$: C 74.14; H 4.42; N 4.55. Found: C 74.09; H 4.51; N 4.61. ^{1}H NMR (300 MHz, $(CD_3)_2CO$) δ 13.65 (2H, s, Ar–O*H*), 9.29 (2H, s, *H*C═N), 8.57 (2H, d, Ar-*H*), 8.24 (2H, dd, Ar-*H*), 8.07 (4H, m, Ar-*H*), 7.58 (2H, m, Ar-*H*), 7.50 (4H, m, Ar-*H*), 7.32 (6H, m, Ar-*H*), 7.21 (2H, d, Ar-*H*). IR (ATR) $\nu_{C=O}$ (ester) 1723 cm^{-1}, $\nu_{C=N}$ (imine) 1610 cm^{-1}.

*N,N′-Bis(5-(2′-naphthoxycarbonyl)salicylidene)-1,2-phenylenediamine (**6b**).* Yield: 92%. Elemental analysis calcd (%) for $C_{42}H_{28}N_2O_6{\cdot}0.5H_2O$: C 75.78; H 4.39; N 4.21. Found: C 75.67; H 4.33; N 4.52. ^{1}H NMR (300 MHz, $(CD_3)_2CO$) δ 13.68 (2H, s, Ar–O*H*), 9.20 (2H, s, *H*C═N), 8.59 (2H, d, Ar-*H*), 8.32 (2H, dd, Ar-*H*), 8.00 (6H, m, Ar-*H*), 7.83 (2H, d, Ar-*H*), 7.56 (10H, m, Ar-*H*), 7.21 (2H, d, Ar-*H*). IR (ATR) $\nu_{C=O}$ (ester) 1728 cm^{-1}, $\nu_{C=N}$ (imine) 1616 cm^{-1}.

*N,N′-Bis(5-(2′-naphthoxycarbonyl)salicylidene)-1,2-naphthalenediamine (**6b**′).* Yield: 80%. Elemental analysis calcd (%) for $C_{46}H_{30}N_2O_6{\cdot}H_2O$: C 76.23; H 4.45; N 3.87. Found: C 75.91; H 4.31; N 4.05. ^{1}H NMR (300 MHz, $(CD_3)_2CO$) δ 13.55 (2H, s, Ar-O*H*), 9.35 (2H, s, *H*C═N), 8.69 (2H, d, Ar-*H*), 8.29 (2H, dd, Ar-*H*), 8.02 (10H, m, Ar-*H*), 7.85 (2H, d, Ar-*H*), 7.59 (6H, m, Ar-*H*), 7.50 (2H, dd, Ar-*H*), 7.23 (2H, d, Ar-*H*). IR (ATR) $\nu_{C=O}$ (ester) 1722 cm^{-1}, $\nu_{C=N}$ (imine) 1622 cm^{-1}.

*N,N′-Bis(5-(pentafluorophenoxycarbonyl)salicylidene)-1,2-phenylenediamine (**6c**).* Yield: 89%. Elemental analysis calcd (%) for $C_{34}H_{14}F_{10}N_2O_6$: C 55.45; H 1.92; N 3.80. Found: C 55.58; H 1.57; N 3.89. ^{1}H NMR (300 MHz, $(CD_3)_2CO$) δ 13.55 (2H, s, Ar–O*H*), 9.21 (2H, s, *H*C═N), 8.60 (2H, d, Ar-*H*), 8.32 (2H, dd, Ar-*H*), 7.59 (4H,m, Ar-*H*), 7.22 (2H, d, Ar-*H*). IR (ATR) $\nu_{C=O}$ (ester) 1743 cm^{-1}, $\nu_{C=N}$ (imine) 1615 cm^{-1}.

*N,N′-Bis(5-(pentafluorophenoxycarbonyl)salicylidene)-1,2-naphthalenediamine (**6c**′).* Yield: 76%. Elemental analysis calcd (%) for $C_{38}H_{16}F_{10}N_2O_6$: C 58.03; H 2.05; N 3.56. Found: C 58.04; H 1.84; N 3.68. ^{1}H NMR (300 MHz, $(CD_3)_2CO$) δ 13.55 (2H, s, Ar–O*H*), 9.33 (2H, s, *H*C═N), 8.65 (2H, d, Ar-*H*), 8.32 (2H, dd, Ar-*H*), 8.09 (4H, s + m, Ar-*H*), 7.55 (2H, m, Ar-*H*), 7.25 (2H, d, Ar-*H*). IR (ATR) $\nu_{C=O}$ (ester) 1748 cm^{-1}, $\nu_{C=N}$ (imine) 1614 cm^{-1}.

*N,N′-Bis(5-(p-nitrophenoxycarbonyl)salicylidene)-1,2-phenylenediamine (**6d**).* The above procedure was slightly modified: ethanol was used as the solvent, and the reaction medium was refluxed for 4 h 30 min. After filtration, the orange solid was washed with ethanol and dried with diethyl ether. Yield: 82%. Elemental analysis calcd (%) for $C_{34}H_{22}N_4O_{10}{\cdot}0.5H_2O$: C 62.29; H 3.54; N 8.55. Found: C 62.28; H 3.14; N 8.60. ^{1}H NMR (300 MHz, $(CD_3)_2CO$) δ 13.55 (2H, s, Ar-O*H*), 9.20 (2H, s, *H*C═N), 8.66 (2H, d, Ar-*H*), 8.37 (4H, d, Ar-*H*), 8.17 (2H, dd, Ar-*H*), 7.62 (6H, d, Ar-*H*), 7.50 (2H, m, Ar-*H*), 7.12 (2H, d, Ar-*H*). IR (ATR) $\nu_{C=O}$ (ester) 1728 cm^{-1}, $\nu_{C=N}$ (imine) 1613 cm^{-1}.

*General Procedure for the Preparation of Al^{III} Complexes **7a**′, **7b**–**b**′, **7c**–**c**′, and **7d**.* The corresponding Schiff base (0.1 mmol) was suspended in 5 mL of EtOH. To this yellow suspension was slowly added the solution of $Al(NO_3)_3{\cdot}9H_2O$ (1 equiv in 5 mL of EtOH). The resulting solution became clearer. After being stirred for 3 h at reflux temperature, the resulting solution without any solid in suspension was evaporated to dryness to obtain a dry yellow-orange oil. This oil was triturated with diethyl ether. A solid as powder was recovered by filtration and dried under vacuum.

*N,N′-Bis(5-(phenoxycarbonyl)salicylidene)-1,2-naphthalenediamine Aluminum(III) Nitrate (**7a**′).* Yield: 97%. Elemental analysis calcd (%) for $C_{38}H_{28}N_3O_{11}Al{\cdot}4H_2O$: C 56.93; H 4.53; N 5.24. Found: C 56.88; H 4.54; N 5.54. ^{1}H NMR (300 MHz, $(CD_3)_2SO$) δ 9.78 (2H, s, *H*C═N), 8.78 (2H, br s, Ar-*H*), 8.71 (2H, br d, Ar-*H*), 8.24 (2H, dd, Ar-*H*), 8.00 (2H, m, Ar-*H*), 7.66 (2H, m, Ar-*H*), 7.52 (4H, m, Ar-*H*), 7.34 (6H, m, Ar-*H*), 7.17 (2H, d, Ar-*H*). IR (ATR) $\nu_{C=O}$ (ester) 1709 cm^{-1}, $\nu_{C=N}$ (imine) 1609 cm^{-1}.

*Synthesis of N,N′-Bis(5-(2′-naphthoxycarbonyl)-salicylidene)-1,2-phenylenediamine Aluminum(III) Nitrate (**7b**).* Yield: 92%. Elemental analysis calcd (%) for $C_{42}H_{30}N_3O_{11}Al{\cdot}2H_2O$: C 61.84; H 4.20; N 5.15. Found: C 61.51; H 4.25; N 5.54. ^{1}H NMR (300 MHz, $(CD_3)_2SO$) δ 9.62 (2H, s, *H*C═N), 8.75 (2H, br s, Ar-*H*), 8.28 (4H, br m, Ar-*H*), 8.04 (6H, m, Ar-*H*), 7.85 (2H, br s, Ar-*H*), 7.60 (6H, m, Ar-*H*), 7.49(2H, d, Ar-*H*), 7.18 (2H, d, Ar-*H*). IR (ATR) $\nu_{C=O}$ (ester) 1723 cm^{-1}, $\nu_{C=N}$ (imine) 1617 cm^{-1}.

dx.doi.org/10.1021/ic201208c | *Inorg. Chem.* 2012, 51, 1309–1318

*Synthesis of N,N′-Bis(5-(2′-naphthoxycarbonyl)-salicylidene)-1,2-naphthalenediamine Aluminum(III) Nitrate (**7b′**).* Yield: 80%. Elemental analysis calcd (%) for $C_{46}H_{32}N_3O_{11}Al{\cdot}5H_2O$: C 60.07; H 4.60; N 4.57. Found: C 60.24; H 4.56; N 4.87. ^{1}H NMR (300 MHz, $(CD_3)_2SO$) δ 9.81 (2H, s, *H*C═N), 8.78 (4H, d, Ar-*H*), 8.28 (2H, dd, Ar-*H*), 8.04 (8H, m, Ar-*H*), 7.87 (2H, d, Ar-*H*), 7.59 (8H, m, Ar-*H*), 7.20 (2H, dd, Ar-*H*). IR (ATR) $\nu_{C=O}$ (ester) 1720 cm^{-1}, $\nu_{C=N}$ (imine) 1609 cm^{-1}.

*Synthesis of N,N′-Bis(5-(pentafluorophenoxycarbonyl)-salicylidene)-1,2-phenylenediamine Aluminum(III) Nitrate (**7c**).* Yield: 78%. Elemental analysis calcd (%) for $C_{34}H_{16}F_{10}N_3O_{11}Al$: C 47.51; H 1.88; N 4.89. Found: C 47.68; H 1.76; N 5.00. ^{1}H NMR (300 MHz, $(CD_3)_2SO$) δ 9.61 (2H, s, *H*C═N), 8.75 (2H, d, Ar-*H*), 8.24 (4H, m, Ar-*H*), 7.64 (2H, m, Ar-*H*), 7.18 (2H, d, Ar-*H*). IR (ATR) $\nu_{C=O}$ (ester) 1746 cm^{-1}, $\nu_{C=N}$ (imine) 1619 cm^{-1}.

*Synthesis of N,N′-Bis(5-(pentafluorophenoxycarbonyl)-salicylidene)-1,2-naphthalenediamine Aluminum(III) Nitrate (**7c′**).* Yield: 74%. Elemental analysis calcd (%) for $C_{38}H_{18}F_{10}N_3O_{11}Al{\cdot}H_2O$: C 49.21; H 2.17; N 4.53. Found: C 48.89; H 2.13; N 4.72. ^{1}H NMR (300 MHz, $(CD_3)_2CO$) δ 9.80 (2H, s, *H*C═N), 8.78 (4H, d, Ar-*H*), 8.27 (2H, dd, Ar-*H*), 8.01 (2H, m, Ar-*H*), 7.69 (2H, m, Ar-*H*), 7.21 (2H, d, Ar-*H*). IR (ATR) $\nu_{C=O}$ (ester) 1753 cm^{-1}, $\nu_{C=N}$ (imine) 1609 cm^{-1}.

*Synthesis of N,N′-Bis(5-(p-nitrophenoxycarbonyl)-salicylidene)-1,2-phenylenediamine Aluminum(III) Nitrate (**7d**).* Yield: 86%. Elemental analysis calcd (%) for $C_{34}H_{24}N_5O_{15}Al{\cdot}3H_2O$: C 49.58; H 3.67; N 8.50. Found: C 49.18; H 3.35; N 8.79. ^{1}H NMR (300 MHz, $(CD_3)_2SO$) δ 9.65 (2H, s, *H*C═N), 8.75 (2H, d, Ar-*H*), 8.42 (4H, d, Ar-*H*), 8.33 (4H, m, Ar-*H*), 7.66 (6H, m, Ar-*H*), 7.21 (2H, d, Ar-*H*). IR (ATR) $\nu_{C=O}$ (ester) 1729 cm^{-1}, $\nu_{C=N}$ (imine) 1614 cm^{-1}.

Spectroscopic Measurements. UV−vis spectra were obtained from a Perkin-Elmer Lambda 35 spectrophotometer. Measurements were made in 1 cm path length quartz cells at 293 K. Emission spectra were measured using a Horiba-Jobin Yvon FluoroMax-4 spectrofluorimeter, equipped with three-slit double-grating excitation and emission monochromators. The steady-state luminescence was excited by unpolarized light from a 150 W continuous-wave xenon lamp and detected at an angle of 90° for diluted solution measurements (10 mm quartz cell) by a red-sensitive Hamamatsu R228 photomultiplier tube. Spectra were reference-corrected for both the excitation source light-intensity variation (lamp and grating) and the emission spectral response (detector and grating). The quantum yields for fluorescence in solution were determined using an aqueous solution of quinine sulfate in 1 N H_2SO_4. Concentrations of the solutions, including solutions of standard, were adjusted so that the absorbance at λ_{ex} was between 0.04 and 0.05. In this case, intensity of the measured emission can be considered to be proportional to the concentration of the species in solution. The emission quantum yields were then calculated using eq 1, where ϕ_s is the emission quantum yield of the sample, ϕ_{std} is the emission quantum yield of the standard, A_{std} and A_s represent the absorbance of the standard and the sample at the excitation wavelength, while $\int I_{std}$ and $\int I_s$ are the integrals of the corrected emission envelopes of the standard and the sample, respectively, and η is the refractive index of the solvents used for the samples and standard solutions.

$$\phi_s = \phi_{std}\left(\frac{A_{std}}{A_s}\right)\left(\frac{\int I_s}{\int I_{std}}\right)\left(\frac{\eta_s}{\eta_{std}}\right)^2 \quad (1)$$

^{1}H NMR spectra were recorded using a ARX250 or a DPX300 Brüker spectrometers with working frequencies, respectively, at 250 and 300 MHz for ^{1}H. Chemical shifts were referenced to the residual proton resonance of the deuterated solvents. IR spectra were recorded in the 4000−600 cm^{-1} region with a Perkin-Elmer Spectrum 100 FTIR using the ATR mode.

Electrochemistry Measurements. Square wave voltammetric measurements were carried out with a potentiostat Autolab PGSTAT100. Experiments were performed at room temperature in an homemade airtight three-electrode cell connected to a vacuum/argon line. The reference electrode consisted of a saturated calomel electrode (SCE) separated from the solution by a bridge compartment. The counter electrode was a platinum wire of ca. 1 cm^2 apparent surface. The working electrode was a Pt microdisk (0.5 mm diameter). The supporting electrolyte $(nBu_4N)[PF_6]$ (Fluka, 99% puriss electrochemical grade) and acetonitrile were used as received. The solutions used during the electrochemical studies were typically 10^{-3} mol L^{-1} in complex and 0.1 mol L^{-1} in supporting electrolyte. Before each measurement, the solutions were degassed by bubbling Ar and the working electrode was polished with a polishing machine (Presi P230). Potentials are given vs the Fc^+/Fc couple as internal standard ($E_{1/2}$ = 0.4 V/SCE)

Estimation of the HOMO/LUMO Energy Levels. The energies of the HOMO and LUMO were calculated by using a reported procedure.[30] According to this reference, the value for ferrocene (Fc) with respect to the zero vacuum level is estimated as −4.8 eV, determined from −4.6 eV for the standard electrode potential $E°$ of a normal hydrogen electrode (NHE) on the zero vacuum level, and 0.2 V for Fc versus NHE. The values for the HOMO and LUMO levels were then, respectively, obtained through eqs 2 and 3 as follows:

$$\text{HOMO} = -(E_{ox} + 4.8)\ \text{eV} \quad (2)$$

$$\text{LUMO} = -(E_{red} + 4.8)\ \text{eV} \quad (3)$$

Data Collection and Structure Determination. Intensity data were collected at low temperature on a Gemini Oxford Diffraction diffractometer using a graphite-monochromated Cu Kα radiation source and equipped with an Oxford Cryosystems cryostream cooler device. Structures were solved by direct methods using SUPERFLIP,[31] and refined by full-matrix least-squares procedures on F using the programs of the PC version of CRYSTALS.[32] Atomic scattering factors were taken from the International Tables for X-ray Crystallography.[33] All non-hydrogen atoms were refined anisotropically. Hydrogen atoms were located in a difference map (those attached to carbon atoms were repositioned geometrically), and then refined using a riding model. For compound **7a**, a disorder was observed for an ethanol molecule and a NO_3^- anion, with occupancy of 50% for each part. CCDC-823562 (**7a**) and 823563 (**7d**) contain the supplementary crystallographic data for this paper. These cif data can be obtained free of charge from the Cambridge Crystallographic Data Center via www.ccdc.cam.ac.uk/data_request/cif.

Computational Details. All the calculations described here were carried out with the Gaussian 09 package.[34] The 6-31G(d)

dx.doi.org/10.1021/ic201208c | Inorg. Chem. 2012, 51, 1309−1318

basis set was used for all calculations.[35,36] Molecular geometries of **7a**−**d** and **7a′**-**b′** were optimized in a vacuum without symmetry restraint using DFT method with the B3LYP[37,38] hybrid exchange correlation functional implemented in the Gaussian suite of program. For all schemes the ground state minima have been confirmed by determination of the vibrational frequencies. The electronic transition energies, oscillator strengths, and excited-state compositions were computed by the time-dependent density functional theory method (TD-DFT)[39] using the same functional and basis sets as for the geometry optimization. Solvent effects on transition energies were evaluated by means of the polarizable continuum model (PCM) in its integral equation formalism,[40] and the default parameters were taken from the literature.[34] In the PCM model, the calculation is performed in the presence of a solvent (here MeOH) by placing the solute in a cavity within the solvent reaction field.

■ ASSOCIATED CONTENT

Ⓢ Supporting Information

Square wave voltamogramms for **7a**−**c** and **7a′**−**c′**. Optimized structures for compounds **7a** and **7d**. Frontier molecular orbitals for geometries **7a**, **7a′**, **7b**, **7b′**, **7c**, **7d** calculated by TD-DFT at the B3LYP/6-31G(d) level of theory using Gaussian 09. Cartesian coordinates of the optimized geometries for **7a**, **7a′**, **7b**, **7b′**, **7c**, **7d**. Supplementary X-ray crystallographic data in CIF format. This material is available free of charge via the Internet at http://pubs.acs.org.

■ AUTHOR INFORMATION

Corresponding Author

*E-mail: sutter@lcc-toulouse.fr (J.-P.S); virginie.bereau@iut-tlse3.fr (V.B.).

■ ACKNOWLEDGMENTS

The authors thank Dr. Christine Lepetit (LCC Toulouse, France) for assistance with the DFT calculations and for helpful discussions.

■ REFERENCES

(1) Kleij, A. W. *Eur. J. Inorg. Chem.* **2009**, 193.
(2) Vigato, P. A.; Tamburini, S. *Coord. Chem. Rev.* **2004**, *248*, 1717.
(3) Monsaert, S.; Ledoux, N.; Drozdzak, R.; Verpoort, F. *J. Polym. Sci., Part A: Polym. Chem.* **2010**, *48*, 302.
(4) Du, H.; Pang, X.; Yu, H.; Zhuang, X.; Chen, X.; Cui, D.; Wang, X.; Jing, X. *Macromolecules* **2008**, *40*, 1904.
(5) Zhang, W.; Loebach, J. L.; Wilson, S. R.; Jacobsen, E. N. *J. Am. Chem. Soc.* **1990**, *112*, 2801.
(6) Cozzi, P. G. *Chem. Soc. Rev.* **2004**, *33*, 410.
(7) Morisige, K. *Anal. Chim. Acta* **1974**, *72*, 295.
(8) Morisige, K. *J. Inorg. Nucl. Chem.* **1978**, *40*, 843.
(9) Morisige, K. *Anal. Chim. Acta* **1980**, *121*, 301.
(10) Cozzi, P. G.; Dolci, L. S.; Garelli, A.; Montalti, M.; Prodi, L.; Zacheroni, N. *New. J. Chem.* **2003**, *27*, 692.
(11) Hwang, K. Y.; Kim, H.; Lee, Y. S.; Lee, M. H.; Do, Y. *Chem.—Eur. J.* **2009**, *15*, 6478.
(12) Béreau, V.; Jubéra, V.; Arnaud, P.; Kaiba, A.; Guionneau, P.; Sutter, J.-P. *Dalton Trans.* **2010**, *39*, 2070.
(13) Briggs, M. S. J.; Fossey, J. S.; Richards, C. J.; Scott, B.; Whateley, J. *Tetrahedron Lett.* **2002**, *43*, 5169.
(14) Kashanian, S.; Gholivand, M. B.; Ahmadi, F.; Taravati, A.; Hosseinzadeh Colagar, A. *Spectrochim. Acta, Part A* **2007**, *67*, 472.
(15) Gündüz, S. B.; Küçükkolbaşý, S.; Atakol, O.; Kýlýç, E. *Spectrochim. Acta, Part A* **2005**, *61*, 913.
(16) Huh, J. O.; Lee, M. H.; Jang, H.; Hwang, K. Y.; Lee, J. S.; Kim, S. H.; Do, Y. *Inorg. Chem.* **2008**, *47*, 6566.
(17) Hwang, K. Y.; Lee, M. H.; Jang, H.; Sung, Y.; Lee, J. S.; Kim, S. H.; Do, Y. *Dalton Trans.* **2008**, 1818.
(18) Tang, C. W.; VanSlyke, S. A. *Appl. Phys. Lett.* **1987**, *51*, 913.
(19) Montes, V. A.; Pohl, R.; Shinar, J.; Anzenbacher, P. Jr. *Chem.—Eur. J.* **2006**, *12*, 4523.
(20) Liao, S.-H.; Shiu, J.-R.; Liu, S.-W.; Yeh, S.-J.; Chen, Y.-C.; Chen, C.-T.; Chow, T. J.; Wu, C.-I. *J. Am. Chem. Soc.* **2009**, *131*, 763.
(21) Zhao, H.; Thurkauf, A. *Synth. Commun.* **2001**, *31*, 1921.
(22) Ren, Y.; Himmeldirk, K.; Chen, X. *J. Med. Chem.* **2006**, *49*, 2829.
(23) Dodo, K.; Minato, T.; Noguchi-Yachide, T.; Suganuma, M.; Hashimoto, Y. *Bioorg. Med. Chem.* **2008**, *16*, 7975.
(24) Maes, D.; Riveiro, M. E.; Shayo, C.; Davio, C.; Debenedetti, S.; De Kimpe, N. *Tetrahedron* **2008**, *64*, 4438.
(25) Shinozuka, T.; Yamamoto, Y.; Hasegawa, T.; Saito, K.; Naito, S. *Tetrahedron Lett.* **2008**, *49*, 1619.
(26) Park, W.; Lim, D. *Bioorg. Med. Chem. Lett.* **2009**, *19*, 614.
(27) $BaMnO_4$ is commercially available and easy to handle and requires no activation; which makes it particulary useful for large-scale reactions.
(28) Ikeda, C.; Ueda, S.; Nabeshima, T. *Chem. Commun.* **2009**, 2544.
(29) La Deda, M.; Aiello, I.; Grisolia, A.; Ghedini, M.; Amatib, M.; Lelj, F. *Dalton Trans.* **2006**, 330.
(30) Pommerehne, J.; Vestweber, H.; Guss, W.; Mahrt, R.; Bässler, H.; Porsch, M.; Daub, J. *Adv. Mater.* **1995**, *7*, 551.
(31) Palatinus, L.; Chapuis, G. *J. Appl. Crystallogr.* **2007**, *40*, 786.
(32) Betteridge, P. W.; Carruthers, J. R.; Cooper, R. I.; Prout, K.; Watkin, D. J. *J. Appl. Crystallogr.* **2003**, *36*, 1487.
(33) *International Tables for X-ray Crystallography*; Kynoch Press: Birmingham, U.K., 1974; *IV*.
(34) Frisch, M. J.; Trucks, G. W.; Schlegel, H. B.; Scuseria, G. E.; Robb, M. A.; Cheeseman, J. R.; Scalmani, G.; Barone, V.; Mennucci, B.; Petersson, G. A.; Nakatsuji, H.; Caricato, M.; Li, X.; Hratchian, H. P.; Izmaylov, A. F.; Bloino, J.; Zheng, G.; Sonnenberg, J. L.; Hada, M.; Ehara, M.; Toyota, K.; Fukuda, R.; Hasegawa, J.; Ishida, M.; Nakajima, T.; Honda, Y.; Kitao, O.; Nakai, H.; Vreven, T.; Montgomery, J. A., Jr.; Peralta, J. E.; Ogliaro, F.; Bearpark, M.; Heyd, J. J.; Brothers, E.; Kudin, K. N.; Staroverov, V. N.; Kobayashi, R.; Normand, J.; Raghavachari, K.; Rendell, A.; Burant, J. C.; Iyengar, S. S.; Tomasi, J.; Cossi, M.; Rega, N.; Millam, J. M.; Klene, M.; Knox, J. E.; Cross, J. B.; Bakken, V.; Adamo, C.; Jaramillo, J.; Gomperts, R.; Stratmann, R. E.; Yazyev, O.; Austin, A. J.; Cammi, R.; Pomelli, C.; Ochterski, J. W.; Martin, R. L.; Morokuma, K.; Zakrzewski, V. G.; Voth, G. A.; Salvador, P.; Dannenberg, J. J.; Dapprich, S.; Daniels, A. D.; Farkas, Ö.; Foresman, J. B.; Ortiz, J. V.; Cioslowski, J.; Fox, D. J. *Gaussian 09, Revision A.1*; Gaussian: Wallingford, CT, 2009.
(35) Lee, C.; Yang, W.; Parr, R. G. *Phys. Rev. B* **1998**, *37*, 785.
(36) Stephens, P. J.; Devlin, F. J.; Chabalowski, C. F.; Frisch, M. J. *J. Phys. Chem. A.* **1994**, *98*, 11623.
(37) Becke, A. D. *J. Chem. Phys.* **1993**, *98*, 5648.
(38) Lee, C.; Yang, W.; Parr, R. G. *Phys. Rev. B* **1988**, *37*, 785.
(39) Runge, E.; Gross, E. K. *Phys. Rev. Lett.* **1984**, *52*, 997.
(40) Tomasi, J.; Mennucci, B.; Cammi, R. *Chem. Rev.* **2005**, *105*, 2999.